

A unique mechanism generating the knee and the ankle in the local galactic zone

ANTONIO CODINO¹ AND FRANCOIS PLOUIN²

¹⁾ Dipartimento di Fisica dell'Universita di Perugia and INFN, Italy.

²⁾ former CNRS researcher, LLR, Ecole Polytechnique, F-91128 Palaiseau, France.

Abstract

A new, unique mechanism accounting for the knee and the ankle in the energy spectrum of the cosmic radiation is presented. The interplay of the form and strength of the galactic magnetic field, the rising trend of the nuclear cross sections with energy, the position of the solar cavity within the Galaxy and disc size generates knees and ankles of individual ions. The influence of these observational data on the cosmic-ray intensity at Earth is determined by the appropriate simulation of the cosmic-ray trajectories in the galactic volume. The solid and extensive accord between the computed and measured energy spectra of individual ions and of all ions is discussed and emphasized.

1 Introduction

The differential energy spectrum of cosmic rays presents two small but significant deviations, called knee and ankle, at the nominal energies of 3×10^{15} eV and 6×10^{18} eV, respectively. After the first observation of the knee in 1958 (Kulikov et al., 1958) many experiments confirmed, over the decades, the structure of the knee characterized by a specific bend energy, at about 3×10^{13} eV, and a spectral index of 3, above 6×10^{15} eV. Only in recent years, experimentally, has an important step forward been taken by the

Kascade Collaboration (Kampert et al., 2003; Haungs et al., 2004; Antoni et al., 2005) which identified and measured the knees of individual ions in a very large energy band (10^{15} - 10^{17} eV), with relatively small error bars, and accurately charting the characteristic forms of the energy spectra. A vast literature (see, for example, Erlykin, 1996) testifies of the many attempts to explain and clarify these two deviations, over almost fifty years.

One notable aspect of the solution of the knee problem described here is that the explanation of the ankles of individual ions comes as a gratuity, once the knees are accounted for.

Prerequisites to comprehend the present study may be found in a series of previous works regarding the method of calculation (Codino, Brunetti and Menichelli, 1995; Brunetti and Codino, 2000, Paper I) and the notion of galactic basin (Codino and Plouin, 2003; Codino and Plouin, 2006, Paper II) largely employed in the present study. Section 7 describes an important, new inference, based on observational facts, which relates the knee energy to the ankle energy of the individual ions. This inference is a cross-check, independent from the method of calculation and the notion of galactic basin, that the mechanism generating the ankle and the knee described here is correct.

Due to the limited size of the present paper some collateral aspects of the explanation of the knees are omitted; among these: (1) how the agreement with the experimental data is affected by the particular values of the spectral indices and elemental composition of cosmic ions. (2) Implications and justification of the hypothesis of adopting constant spectral indices over the entire energy interval of the cosmic radiation, i.e. 10^{10} - 10^{21} eV. (3) Direct, important consequences of this solution of the knee problem in our discipline. For instance, according to this study, any acceleration mechanisms in the Galaxy are extraneous to the origin of the knees and ankles. Another notable consequence is that the extragalactic component of cosmic rays is likely to be marginal even at 10^{20} eV. (4) Bibliography of previous attempts to explain the knee reported elsewhere (Codino and Plouin, 2006 Paper III).

2 Evaluating cosmic ray intensity using cosmic ray trajectories

In order to evaluate the cosmic ray intensity in a given small volume of the Galaxy, for example the solar cavity, the number of cosmic ray trajectories

intercepting it has to be computed. Trajectories are just the physical paths of cosmic rays determined by computer simulation. The initial point of any trajectory is the source while the final point is the site where the cosmic ion disappears from the disk. Nuclear collisions, ionization energy losses and escape from the disc are the three causes that make cosmic rays disappear from the disc.

The following astronomical, astrophysical and radioastronomy observations, are incorporated in the computational algorithms: (1) the spiral field pattern shown in figure 1; (2) the magnetic field strength (see figure 4 in Paper II); (3) the form and the dimension of the Galaxy (see figure 1 in Paper I); (4) a uniform distribution of cosmic ray sources in the galactic disk (see eqn. (5) in Paper I); (5) the nuclear cross sections ion-hydrogen, σ ; (6) the interstellar matter density in the disk, d , of 1.24 hydrogen atoms per cm^3 (Gaisser, 1990); (7) the position of the solar cavity inside the disk, shown in figure 1, at 14 pc from the galactic midplane.

A cosmic ion emanated from a source travels, on average, a mean length L , in the disk volume, primarily determined by σ , the magnetic field structure and d . Typically, this global length L is subdivided into thousands and thousands of segments, depending on the particular region of propaga-

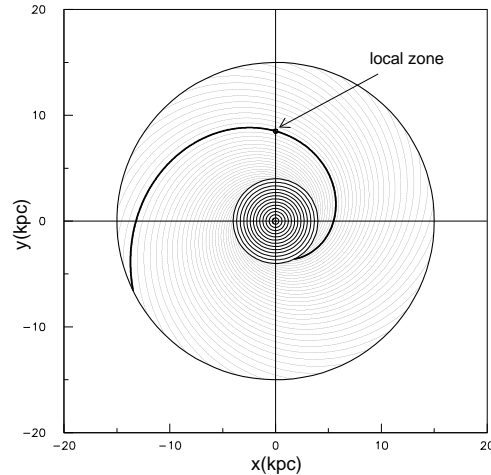


Figure 1: The regular component of the magnetic field in the disk is spiral according to a variety of measurements in our own Galaxy and many other spiral galaxies morphologically similar to the Milky Way. The solid black curve denotes the principal magnetic field line; it is rooted on the bulge edge at $r=4$ kpc terminating at $r=15$ kpc with a length of 40.7 kpc . This particular spiral intercepts the solar cavity at a distance of 8.5 kpc from the galactic center.

Table 1: Shapes and field strengths of the regular magnetic fields in spiral galaxies determined by radio continuum measurements.

Galaxy	Regular field Shape	field strength μG	References
M33	spiral	3 ± 1	Sofue et al. 1981
M51	spiral	10	Mathewson et al. 1972
NGC6946	spiral	12 ± 4	Klein et al. 1982
M81	spiral	8 ± 3	Sofue et al. 1980
M83	spiral	not given	Ondrechen 1985
M31	circular	3-4	Beck 1981
IC342	circular	7 ± 2	Graeve et al. 1988
NGC253	probab. spir.	a few μG	Klein et al. 1983
NGC2903	spiral	not given	Sofue et al. 1985
NGC5055	probab. spir.	not given	Sofue et al. 1985
NGC4631	not given	a few μG	Golla et al. 1988
NGC891	parall. gal. plane	a few μG	Sukumar et al. 1991
NGC4565	parall. gal. plane	not given	Sukumar et al. 1991
NGC3251	spiral	10 μG	Knapik et al. 2000
NGC5055	spiral	9 μG	Knapik et al. 2000

tion and the energy of the cosmic ion. The ion propagation normal to the regular spiral field is generated by the chaotic field leading to a transverse-to-longitudinal displacement ratio of 0.031, value compatible with the quasi-linear theory of ion propagation in an astrophysical environment (Giacalone & Jokipii, 1999). The chaotic magnetic field is materialized by magnetic cloudlets (see, for instance, Vallée, 1998) with variable dimensions and a field strength a factor 3 greater than that of the regular field.

3 Galactic basins around the knee energy region

Most of the cosmic ions wandering in the Galaxy do not intercept any given recording instrument, placed in a specified site in the Galaxy, just because of an abnormal distance source-instrument, or possibly, because of the low probability of encounter, due to the gas density, high nuclear cross sections or magnetic barriers. Generally, only a subset of the cosmic rays emanated by the galactic sources intercepts any given recording instrument. In figure 2 this notable aspect is illustrated. The positions of the sources emitting cosmic rays reaching the local zone are far from being uniformly distributed in

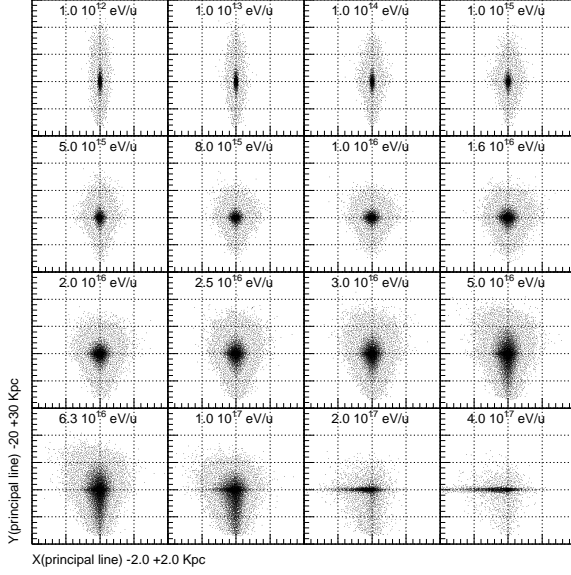


Figure 2: Source distributions for iron nuclei projected onto the galactic midplane at sixteen different energies, from one TeV/u up to the ankle energy region. The spiral reference frame, bound to the principal magnetic field line, is used. Note the different scales in the two axes. The disruption of the source pattern, going from an oval to a squat form as the energy increases, is obvious.

space; on the contrary, they accumulate in particular disk regions, generally in the vicinity of the instrument. In figure 2, sixteen source distributions of iron nuclei, projected onto the galactic midplane, are given for sixteen different energies, from $5.6 \times 10^{14} eV$ up to the ankle energy region.

Figure 3 displays a contour plot encompassing 90% of the sources emitting cosmic rays intercepting the local galactic zone. The contours in figure 3 refer to the same iron source distributions in figure 2 at the two particular (arbitrary) energies of 5.6×10^{14} and $3.5 \times 10^{18} eV$. These particular source patterns delimited by the dotted curve surrounding the recording instrument are called here *galactic basins*. They are only a subset of the total number of sources present in the disk. In this paper the recording instrument is the Earth, also referred to as *local galactic zone* or *solar cavity* (the black dot in figure 1).

Let us emphasize some features of the galactic basins in figure 3. The star outside the iron basin of $10^{12} eV/u$ represents a source. Since this

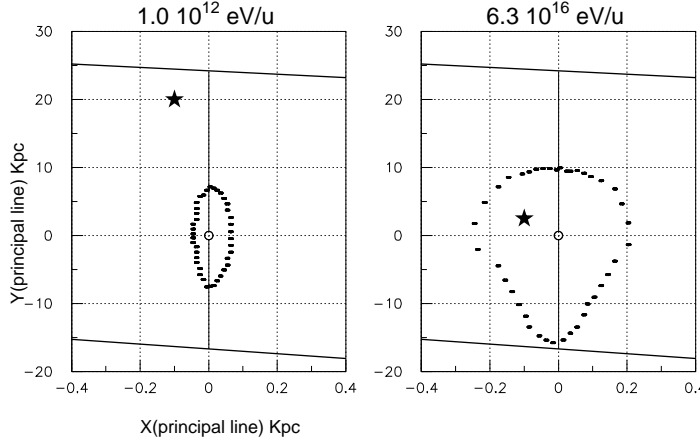


Figure 3: Contour plots containing 90% of iron sources at the energy of 10^{12} and $6.3 \times 10^{16} \text{ eV/u}$ in the spiral reference frame. These contours refer to the same iron samples shown in figure 2 and are called *galactic basins*. The energy of the right contour is between the *knee* and *ankle* energy region. Galactic basins enlarge with increasing energy, going from oval to ram-head shapes. This enlargement causes an increase of the cosmic ray intensity at Earth.

source does not belong to the basin it implies that, on average, cosmic rays emitted from it do not reach the Earth but, more likely, they will abandon the disk, or eventually, they will suffer nuclear collisions in the disk. The star inside the iron basin of $6.3 \times 10^{16} \text{ eV/u}$, on the contrary, emanates cosmic rays that, with a probability higher than 90%, will arrive at Earth. Therefore, this source belongs to the basin.

Generally, cosmic ray intensity registered by a terrestrial instrument has to diminish as the energy increases, above 10^{14} eV , if the number of sources feeding the solar cavity diminishes with increasing energy. There are two competing processes, referred to as α and β , controlling the number of sources powering the flux at Earth: one (α) causing an increase of the flux, another (β) causing a decrease. The basin size increases with energy as clearly displayed in figure 3 where the energy varies from 10^{12} to $6.3 \times 10^{16} \text{ eV/u}$ (see also figure 8, Paper III). As a consequence, the number of sources increases with the energy, resulting in a higher flux (process α). At the same time, as the energy increases, the average length of cosmic ray trajectories in the Galaxy diminishes, implying a decrease of the flux in the local zone (process β). Since the serpentine profile of the trajectories at low energy (see figure 3, Paper I) becomes less and less intricate with increasing energy (reaching the rectilinear propagation at $4 \times 10^{18} \text{ eV}$ for helium),

the probability of intercepting the local galactic zone decreases at higher energies. In fact, intricate trajectories, under the same physical conditions, yield higher fluxes than rectilinear trajectories, as intuition suggests and detailed calculations demonstrate.

The process α , intrinsically, would have yielded a large flux enhancement with increasing energy, at Earth, in the interval 10^{12} - 10^{17} eV, if the thickness of the Galaxy would have been much larger (say, exaggerating, 1000 pc) than its real value of hundreds pc. The small disk thickness boosts the escape probability against the gain in the number of sources (process α), intrinsic to the basin enlargement, as the energy increases. Quantitatively, there is a very small flux enhancement at Earth, as the energy increases between 6×10^{12} and 2×10^{15} eV (5.8% for He), because of the finite disk thickness which erodes the full enhancement effect of the process α .

A third effect, referred to as process γ , is caused by the characteristic trend of the inelastic nuclear cross sections, which rise with energy, making the average trajectory length in the disk shorter, compared to the average length evaluated by constant cross sections. And this effect continuously and permanently influences both processes α and β , discussed above and conceived at constant cross section, for simplicity. The only way to quantify the effect of rising cross sections is to calculate the same physical quantities (intensities, energy spectra etc.) with constant cross sections, chosen at an arbitrary energy (10^{11} eV) and to compare the differences. This will be done in the next Section 4. The relative importance of the processes α , β and γ at different energies creates the knees of the individual ions as will be quantitatively clarified in the next Section.

4 Nuclear collision rate in the whole disk

In the previous Section 3 using the notion of galactic basin and a variety of arguments, a potential fall or rise of the cosmic-ray intensity versus energy has been anticipated at very high energy. Galactic basins specify the clustering of the sources related to the position of a given recording instrument. Galactic basins are just geometrical figures in the disk volume linking the sources and the recording instrument. Generally, the particle flux is not linear with energy. For example, the volume of a galactic basin might be proportional to the flux on a recording instrument, only if a uniform distribution of sources populates the region around the instrument, and eventually, other pertinent phenomena are approximately constant with varying energy.

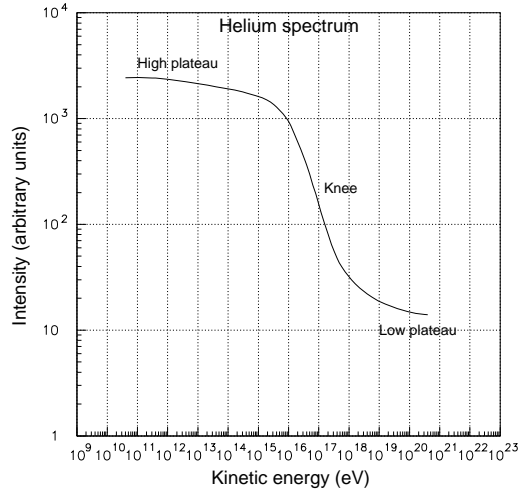


Figure 4: Number of cosmic rays (helium) reaching the local galactic zone n_g versus energy with an arbitrary normalization. The structure of the curve presents a high plateau, a steep descent and a low plateau.

Instead of dissecting the cosmic-ray flux in partial contributions in order to comprehend the origin of the knees in a coherent rational scheme as made in the previous section, it is also useful and complementary to calculate the number of cosmic rays reaching the local galactic zone, hereafter referred to as n_g . This quantity versus energy is shown in figure 4 for helium. Note that a cosmic ion emitted from a source with an energy E_s will reach the local galactic zone with the same energy E_s , since at these high energies ionization energy losses are negligible.

The quantity n_g is approximately proportional to the energy spectrum of the cosmic rays when the spectral index at the sources is taken into account. As apparent from figure 4 the spectrum presents three different regions: (1) a high plateau; (2) a steep descent; (3) a low plateau. Figure 5 reports n_g versus energy, for six ions, representative of important nuclear species.

In order to appreciate the forms of the spectra given in figure 4 and 5 it is useful to determine the number of cosmic rays suffering nuclear collisions in the whole disk for an arbitrary initial sample (several million fully reconstructed cosmic-ray trajectories have been used for the results in figure 5). Cosmic rays either escape from the disk or are destroyed by nuclear colli-

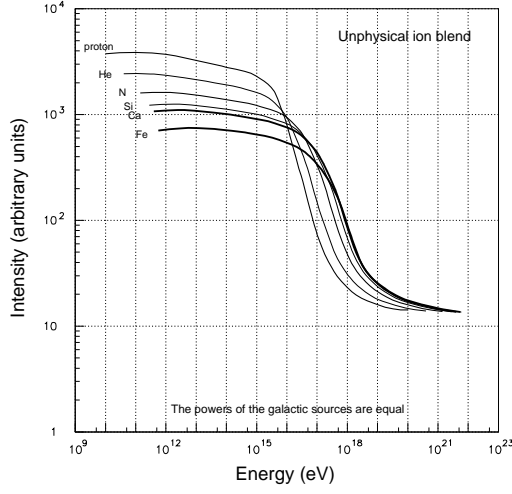


Figure 5: Energy spectra of six nuclear species obtained by ideally assuming equal source powers of any galactic ions (referred to as unphysical ion blend). This unphysical condition visualizes the regularity and smoothness of the spectra for different nuclear species. The differences in the intensities at a given energy are due to the nuclear cross sections and to the different grammages experienced by cosmic ions while propagating in the disc.

sions and the probabilities for the two processes are intimately related. Any given sample of trajectories with sources rooted in the disk volume must satisfy the equation: $f_N + f_E = 1$, where f_N is the fraction of trajectories undergoing nuclear collisions and f_E that escaping from the disk. Note that, at high energy, the fraction of trajectories extinguished by ionization energy losses, f_I , is zero and consequently omitted from the above equation.

The number of nuclear collisions versus energy in the whole disk is shown in figure 6. Curves (a), (b) and (c) refer to helium while the solid black curve to iron. Curve (a) is obtained by the set of parameters mentioned in Section 2 (real, observational parameters) while, for curve (b), the field strength is artificially multiplied by a factor 10, and for curve (c), reduced by a factor 10. Of course, the iron spectrum in figure 6 also splits into three similar curves which, for simplicity, are not shown.

The effect of the magnetic field is to bend and invert particle trajectories during ion propagation in the disk. When this process is at full regime, the matter thickness encountered by cosmic rays (the grammage) is constant and

the resulting number of nuclear collisions is also constant, if nuclear cross sections are constant. The high plateau between 10^{12} and 10^{16} eV for helium and between 10^{13} and 10^{18} eV for iron exhibits this condition. When the bending power of the magnetic field, around 10^{16} eV for helium, becomes inefficient (or less efficient than that of the magnetic field configuration operating at lower energies) trajectories become less and less twisted, and consequently, the probability of escaping from the disk grows. Equivalently stated, the number (or the fraction) of nuclear collisions decreases with increasing energy, and since $f_E = 1 - f_N$, the rate of particle escape increases. Hence, cosmic ray intensity in the disk abruptly reduces and a steep fall appears. But the descent cannot continue indefinitely. Once the magnetic field has completely lost its bending power, so that cosmic ions propagate in straight-line segments, the matter thickness attains its minimum value; in this condition, the low plateau with a constant, minimum number of nuclear collisions is attained. The separation of the energy spectra (a), (b) and (c)

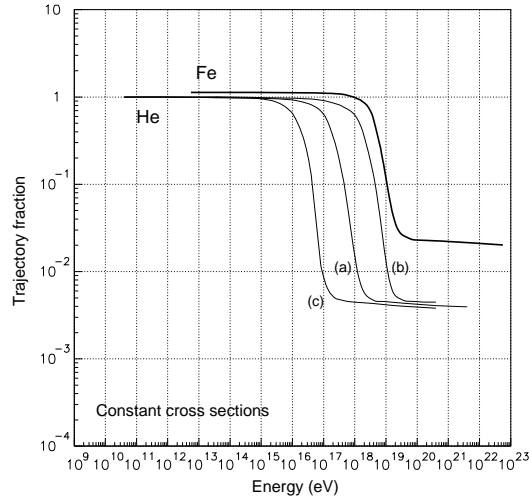


Figure 6: Effect of the magnetic field strength on the nuclear collision rate of helium and iron occurring in the disk. The correct magnetic field strength refers to curve (a) while in curve (b) the strength is artificially enhanced by a factor 10, and curve (c) decreased by a factor 10. Helium-proton and iron-proton nuclear cross sections of 102 mb and 718 mb, respectively, at the arbitrary energy of 100 GeV, are adopted in this particular calculation; they are artificially taken constant in the energy interval 10^{10} - 10^{21} eV, just to single out and quantify the difference on the flux against (real) rising cross sections. Trajectories fractions are normalized to 1 for helium, at the energy of 10^{12} eV.

Table 2: Relative abundances of cosmic ions and spectral indices at the arbitrary energy of 2×10^{15} eV. The ion groupings CNO, Ne-S and Fe(17-26) derive from the traditional data analysis in many experiments. The computed spectral index of the complete spectrum is denoted by γ .

	Blend 1		Blend 2		Blend 3	
	Proton abundant		Proton superabundant		Helium abundant	
Ion	Comp.	Index	Comp.	Index	Comp.	Index
H	32.8%	2.72	37.9%	2.74	19.6%	2.72
He	29.7%	2.72	27.4%	2.72	35.5%	2.72
CNO	11.7%	2.65	10.8%	2.65	14.0%	2.65
Ne-S	10.0%	2.65	9.3%	2.65	12.0%	2.65
Fe(17-26)	15.0%	2.60	13.8%	2.60	17.8%	2.50
Ca	0.8%	2.60	0.8%	2.60	0.1%	2.60
γ		3.05		3.06		3.00

in figure 6 vividly and beautifully manifests how the particular bend energy in the spectrum is controlled by the average magnetic field in the Galaxy. Table 1 firmly attests the experimental basis of the average field strengths in spiral galaxies which, beyond any doubt, fix and delimit along the energy axis, the realm of the rectilinear propagation.

Detailed calculations indicate that the transition from the results shown in figure 6 to those reported in figure 4 and 5 (energy spectra to be compared with the experimental data) is accounted for by the effect of rising cross sections and the position of the local zone in the Galaxy. The similarity of the curves demonstrates that the break of the high plateau caused by the magnetic field is a general phenomenon occurring both in the local zone (a sphere of 50 pc in diameter in this particular calculation) and in the whole disc. The method of calculation used for the results given in figure 6 is described elsewhere (see Section 4, Paper II).

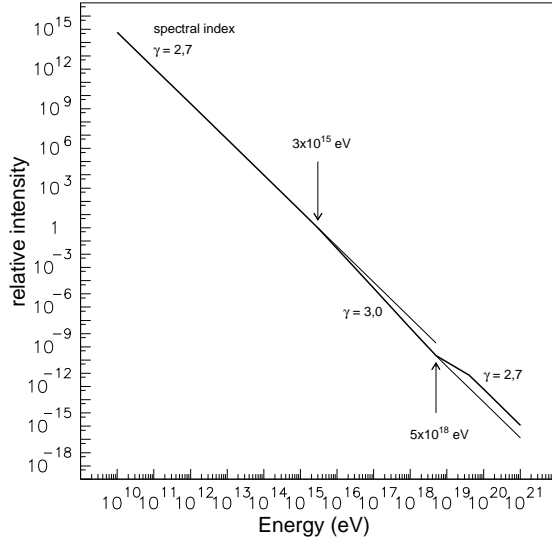


Figure 7: Universal energy spectrum of the cosmic radiation measured at Earth in the interval 10^{10} - 10^{21} eV with the relevant spectral indices, and with knee and ankle energies indicated. The thin line above 3×10^{15} eV is the spectrum extrapolation with an index of 2.7 and that above 5×10^{18} eV is the extrapolation with an index of 3.0. The difference between measured and extrapolated spectra suggests that the *knee* and the *ankle* are small perturbations. The approximate equality of the spectral index over the entire energy range lends credence to the existence of a universal acceleration engine operating inside and outside galaxies as argued elsewhere (Codino, 2005).

5 Computed and measured proton, helium and iron energy spectra

The comparison of the computed energy spectra with the measured ones, in the energy band 10^{15} - 10^{19} eV, although simple and feasible, requires the spectral indices and chemical composition of the individual cosmic ions at the cosmic-ray sources. Figure 7 shows the differential energy spectrum of the cosmic radiation in the interval 10^{10} - 10^{21} eV with some characteristics. In spite of the two significant deviations at 3×10^{15} and 5×10^{18} eV, the spectrum is remarkably linear in the logarithmic scales of intensity and energy. The subsequent analysis of the knees takes advantage of this linearity by assuming constant spectral indices for any ion in the whole energy range

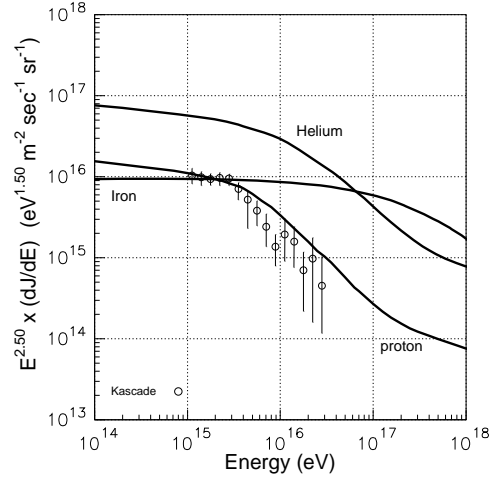


Figure 8: Proton energy spectrum compared with the experimental data measured by the Cascade Collaboration elaborated by the SIBYLL algorithm. The proton spectrum measured by the Tibet AS γ Collaboration (Amenomori, 2006) seems in disagreement with the present evaluation and incompatible with the Cascade outcomes (the bend energy and spectrum form as well).

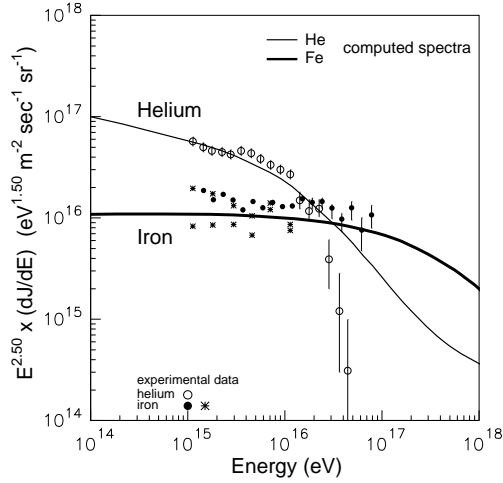


Figure 9: Computed helium and iron energy spectra compared with the experimental data. Open dots (He) and full dots (Fe) from the Cascade Collaboration; stars (Fe) from the Eas-top Collaboration indicate the maximum and minimum intensity at the specified energy.

10^{10} - 10^{21} eV. This ultrasimplified hypothesis is indeed supported by many experimental data (on the absence of a spectral break at low energy see, for example, Cherry, 1999). Notice however, that any other hypothesis, in the form of two or more values of the spectral indices in the energy range 10^{10} - 10^{21} eV would yield an even better agreement in the comparison with the experimental data.

Traditionally, leaky box models of cosmic rays subdivide the spectral index (always close to 2.7) of a nuclear species observed at Earth as the sum of two parts: one due to the sources (typically 2.2) and the rest due to the propagation. The logical necessity for this splitting remains, to date, largely undemonstrated and the observational evidence contradictory, as it results from the comparison of the spectral index at the sources extracted from the analysis of the anisotropy of the arrival direction of high energy cosmic rays (Hillas, 1984) and that extracted from the γ -ray spectrum recently measured by the HESS Collaboration (Aharonian, 2006). Accordingly, the hypothesis for this splitting is not retained. An empirical approach is adopted here, where spectral indices of the individual ions in the whole disk are assumed to be those measured at Earth. *A posteriori* this crude approximation is more than adequate for the explanation of the knees.

In Table 2 are given three elemental compositions and related spectral indices (hereafter called ion blends) at the arbitrary energy of 2×10^{15} eV where the equalization of the computed energy spectra to the experimental ones is imposed.

Let us anticipate here that by altering the values of the ion blends, within plausible limits bound to measurements, the agreement between computed and measured energy spectra substantially persists. Notice, on the contrary, that the spectral indices become critical, for the accord with the data, at energy regions quite remote from the knee energy band (e.g. at the ankle energy region, see subsequent figures 11 and 12). Figure 8 shows the proton energy spectrum with a spectral index of 2.6, based on the Atic experiment, at very low energy (Adams et al., 2005), normalized to the flux of 0.97×10^{-22} particles/eV $m^2 sr sec$, measured by the Kascade Collaboration (Roth et al., 2003) at the energy of 2×10^{15} eV. The computed spectrum conforms fairly well to the measurements; taking a soft spectral index (for example, 2.72) instead of a hard one, the agreement with the experimental data becomes excellent. The energy spectrum obtained by the Sibyll algorithm in Kascade gives a similar accord, since the resulting spectra almost shift in parallel manner in intensity. Note that the mentioned shift in intensity is absorbed in the normalization, so preserving the accord.

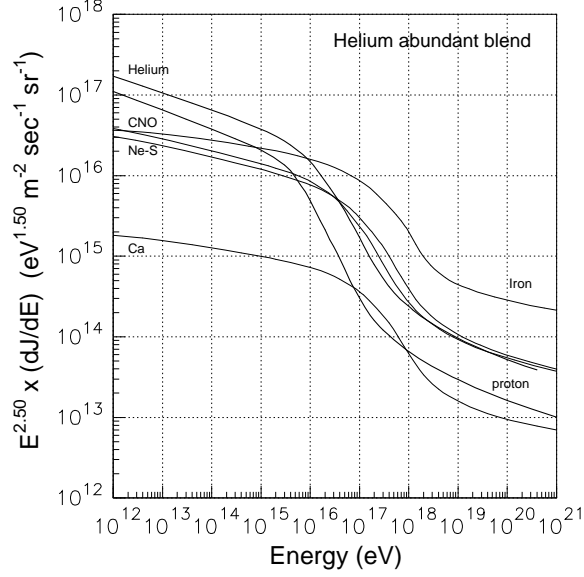


Figure 10: Computed energy spectra of individual ions according to the elemental abundances and spectral indices given in Table 2 referred to as blend 3. These curves are just one of the many examples of how the energy spectra given in figure 5 may be transformed by a particular ion blend.

In figure 9 are given the computed helium and iron spectra (thick lines) compared with the experimental data of Kascade and Eas-top Collaborations (Navarra et al., 2003). In this case, the helium spectral index of 2.72 has been used and the traditional value of 2.5 for iron (Mueller, 1989), as measured at low energy. The helium-to-iron flux ratio of 3.75 at the normalization energy of 2×10^{15} eV has been imposed using the data from the Kascade Collaboration (Roth et al., 2003). Comparing the computed helium spectra in figures 8 and 9 (thick lines in both figures), which have different spectral indices of 2.6 and 2.72, a visual quantification of the general effect of the indices on the intrinsic spectra given in figure 5, may be appreciated. The global agreement with the measured H, He and Fe spectra is more than satisfactory.

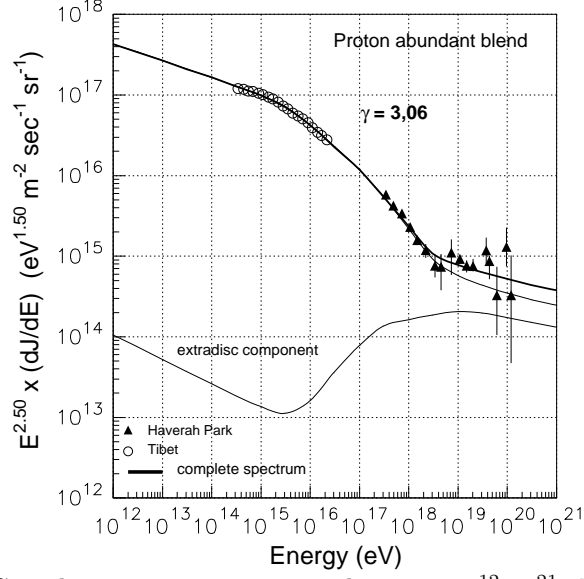


Figure 11: Complete energy spectrum in the range 10^{12} - 10^{21} eV with the ion blend 2 of Table 2 and its comparison with the Tibet and Haverah Park data.

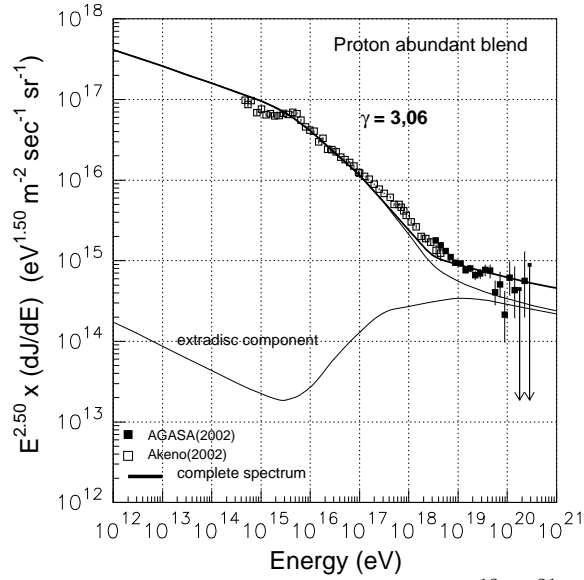


Figure 12: Complete energy spectrum in the range 10^{12} - 10^{21} eV with the ion blend 2 of Table 2 and its comparison with the Akeno and Agasa data.

6 The complete spectrum of the cosmic radiation between the knee and the ankle

The complete spectrum of the cosmic radiation is the sum of the partial spectra of the individual ions. Figure 10 shows an example of partial spectra for six ions. The indices and elemental abundances of these energy spectra are those reported in Table 2, blend 3. The regular, smooth spectra displayed in figure 5, which have (artificial) equal abundances at the sources, transform into those shown in figure 10, which are scattered in intensity, due to the uneven chemical composition and differing spectral indices, ranging from 2.60 to 2.72.

In figures 11 and 12 the complete energy spectra for the ion blend 2, in the interval 10^{10} - 10^{21} eV, are given, along with the data of some groups : Tibet and Haverah Park experiments in figure 11 (Amenomori, 1996; Lawrence, 1990) Akeno and Agasa experiments in figure 12 (Hara, 1979; Nagano, 1992). The computed spectrum is required to agree with the experimental data only at one energy point, at the arbitrary energy of 1.0×10^{16} eV and no other constraint is imposed. For sake of completeness, at the energy of 1.0×10^{16} eV, the intensity ratio of the complete spectra between Tibet and Cascade experiments is taken 1.4 while that between Akeno and Cascade 0.65. The overall accord is fairly good, and in particular, the spectral index γ of 3.06 for this ion blend 2 in the energy interval 6.0×10^{15} - 10^{17} eV is in excellent agreement with the data of the quoted experiments and many others. The other ion blends 1 and 3 give similar results for γ , 3.05 and 3.0, respectively, as reported in Table 2.

In the present investigation of the energy spectrum between the knee and the ankle, the traditional hypothesis (see, for example, Rossi B., 1964) is admitted that a fraction of the sources powering the flux at Earth might not be located in the disc volume. Let us call these sources extradisc rather than extragalactic since there are claims of sources placed in the halo (Hillas, 1998; Dar, 2001; Plaga, 2003). In the next Section it is demonstrated that the expected extradisc flux, if any, has to peak between the energies of 3×10^{18} and 5×10^{19} eV, namely, the minimum (for protons) and maximum energies (for Fe) attesting the rectilinear propagation of cosmic rays in the Milky Way. Incorporating this anticipated result here, the extradisc component (I_e) is normalized at the energy of 1.0×10^{19} eV. The normalization requires that the sum of the extradisc and galactic intensity at Earth (I_g) equals the observed value of 2.5×10^{-33} particles/eV m^2sr sec as measured by

the Haverah Park experiment (figure 11) or by 2.25×10^{-33} particles/ $eV m^2 sr sec$ as measured by Agasa Collaboration (figure 12). It is found that $(I_g + I_e)/I_e$ is about 3.6 in figure 11 and $(I_g + I_e)/I_e$ about 2.5 in figure 12.

The energy spectra of the extradisk component are determined by taking into account the modification of the energy spectra and ion blends (with respect to those given in Table 2) experienced by the galactic cosmic rays overflowing from the Galaxy and the analogous modifications suffered by the extragalactic cosmic rays penetrating the Milky Way from its exterior and reaching the solar cavity. Details of this development will be given at the CRIS Catania Conference 2006 (Codino and Plouin, 2006).

7 How the knee and ankle energies of individual ions are interconnected

Consider the extreme simplified condition of galactic and extragalactic cosmic rays represented in figure 13. Galactic sources are represented by di-

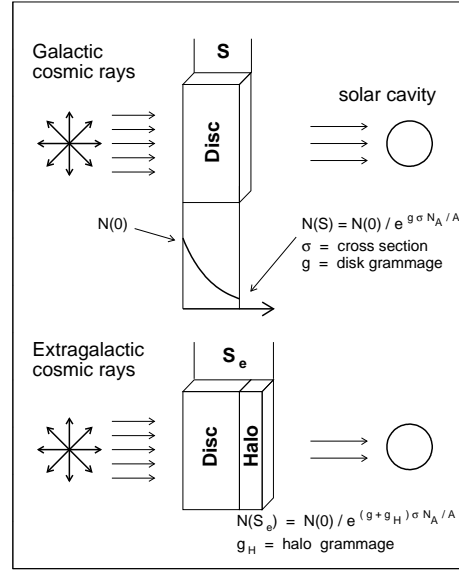


Figure 13: Schematic illustration of galactic and extragalactic sources (sheafs of arrows) contributing to the global flux at the solar cavity (also Earth). The slabs of matter represent the grammage encountered by cosmic ions in the travel to the Earth. The grammage is a global parameter, incorporating the structure of the magnetic field and the dimension and the matter density of the traversed medium.

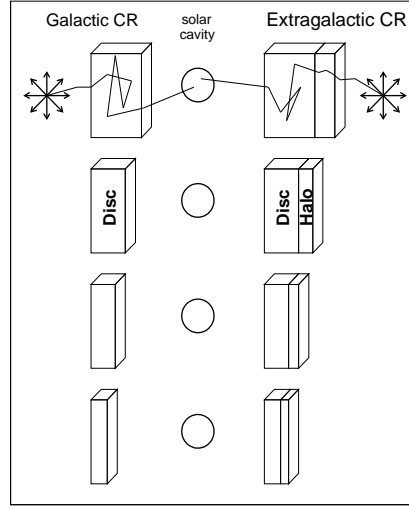


Figure 14: Sequence of barriers of matters (slabs) that galactic and extragalactic cosmic rays should penetrate in order to contribute to the local flux at Earth. The thicknesses of these barriers decrease with increasing energy attaining a minimum value at a particular, distinctive energy, for a given nuclear species. The energy corresponding to this minimum defines the ankle energy.

verging arrows while the disc and halo by slabs of matter with appropriate thicknesses. The slab thickness, s , is the average distance experienced by cosmic rays in the travel from a (fictitious) average disc source to the solar cavity (circle) and likewise s_e for extragalactic cosmic rays. The disc grammage g (in g/cm^2) is defined as mnL where n is the average atomic mass in the disc, n is the number density of atoms, L the mean trajectory length, and likewise g_H for the halo grammage. The corresponding average matter densities experienced by galactic and extragalactic ions are : $d=g/s$ and $d_e=g_H/s_e$, respectively. Note that s and s_e are constant lengths which disappear from the final formulae.

Galactic sources emanate cosmic rays which propagate through the disc and beyond its border. Some of these ions are destroyed by nuclear collisions in the disk, some others evade into the halo, and only a tiny fraction arrives to the solar cavity. Similar partitions of the flux should occur for the extragalactic component (bottom part of figure 13) with the only difference that the slab thickness, s_e , is a bit higher than that experienced by galactic cosmic rays. This is due to the larger size of the traversed medium. The matter densities of these barriers (or the grammages g and g_H) certainly vary with the energy as qualitatively shown in figure 14. Going from low to very high

energy, at about 10^{18} eV, the grammage must reduce to a minimum value which is attained as cosmic rays propagate rectilinearly.

The intensity at Earth of the extragalactic component is simply determined by the nuclear cross section and the grammage. As an example, figure 15 displays the helium-proton cross section, which rises with energy, and the helium grammage g_H versus energy. The average minimum energy at which cosmic rays penetrate unbent the interstellar medium and the halo, marks the onset of the rectilinear propagation and in this condition a minimum grammage is attained. The characteristic energy value at which this occurs, at 4×10^{18} eV for helium, is due to the average strength of the magnetic field in the Milky Way and the charge of the ion.

The number of particles surviving the barrier, those arriving at Earth, is governed by the attenuation length, λ , equal to $A/\sigma d_e N_A$ in the ratio s_e/λ where N_A is the Avogadro number and A the average mass of the galactic atom. The product $s_e \sigma d_e$, or more simply σg_H , has necessarily a minimum, shown in figure 16, because of the forms of the curves shown in figure 15. But the minimum of the barrier density corresponds to the maximum penetration of the barrier, which in turn, translates in an intensity maximum for the extradisc component. Repeating this calculation for iron the intensity maximum is at 5×10^{19} eV. Therefore, in the energy band,

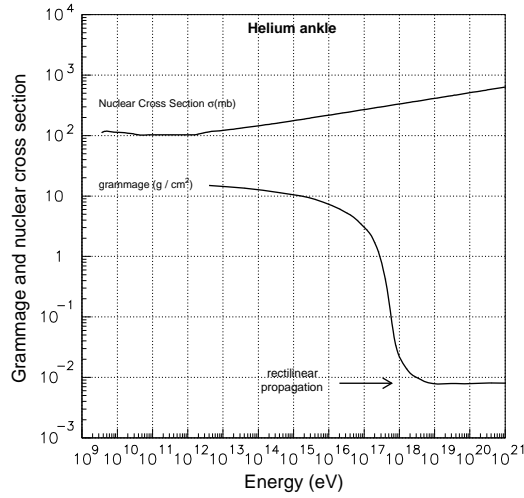


Figure 15: Helium-proton inelastic cross section versus energy (top curve). Helium grammage versus energy (bottom curve) in the galactic disc. The arrow indicates the particular minimum energy of 4×10^{18} eV at which the grammage attains its asymptotic value.

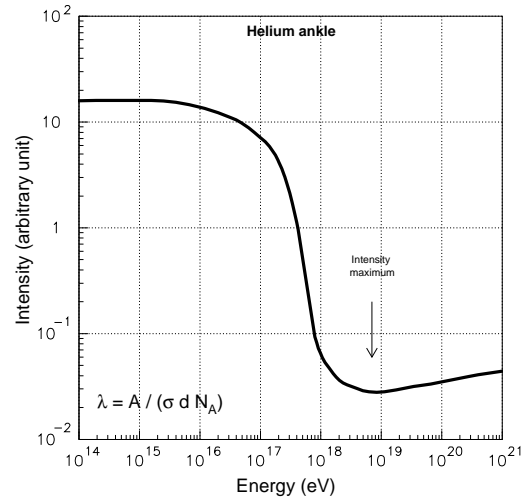


Figure 16: Number of extragalactic cosmic helium ions arriving at Earth with an arbitrary normalization. There is a minimum in the barrier thickness between the extradisc sources and Earth generating the intensity maximum at about 7×10^{18} eV. This minimum is identified with the helium ankle.

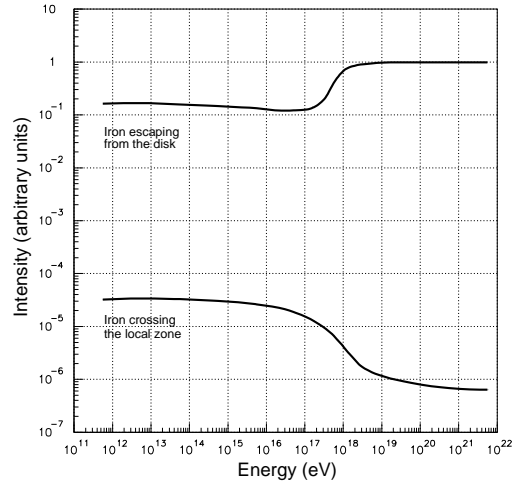


Figure 17: Number of iron nuclei escaping from the disk (top curve) and those intercepting the local galactic zone versus energy. An iron knee and antiknee appear as a result of the different positions in the Galaxy of the two recording instruments. The relative intensities of the two curves, based on 4×10^5 simulated trajectories, are arbitrarily normalized. The computed iron knee (bottom curve) is the same spectrum shown in figure 9 in accord with the Kascade and Eas-top data.

from 3×10^{18} to 5×10^{19} eV an intensity maximum is expected, being the ankle energy for protons at about 3×10^{18} eV, a bit lower than that of helium at 7×10^{18} eV. Accurate measurements of the Hires Collaboration in the energy band 10^{18} - 10^{20} eV do actually indicate an intensity bump in this region (Springer et al., 2003). Other experiments (Haverah park, Yakutsk, Agasa) register a similar intensity bump with respect to the extrapolation of the spectrum, at constant spectral index, measured at lower energies, below 10^{18} eV. This inference and the conclusion for the existence of an intensity bump are independent, within plausible empirical limits, from the ion blend and the spectral indices of the extragalactic component, and to a large extent, from the method of calculation.

8 Conclusions

The uneven efficiency of the magnetic field to retain cosmic rays in the Galaxy at high energies, above 10^{13} eV, is insufficient to account for the knees of the individual ions and for the knee. This decreasing efficiency would yield an enhancement or a depression of the flux at Earth, depending on the nuclear species and the particular energy. It is only by the detailed analysis of the effects of nuclear cross sections, the position of the solar cavity and the disc size on cosmic ray flux at Earth that the origin of the knees and ankles becomes fully comprehensible. Figure 17 shows the number of galactic iron nuclei n_g crossing the disc border (top curve) and that of galactic iron nuclei reaching the Earth (bottom curve) versus energy, exactly in the same conditions. The break of n_g caused by the magnetic field occurs, in both cases, precisely around and above 10^{17} eV, but the effect on the iron intensity measurable by a terrestrial or a peripheral instrument is opposite: in one case there is a knee, in the other an antiknee. This behavior vividly illustrates the importance of the position of the Earth within the Galaxy.

Let us summarize the features of the solution of the knee and ankle problem presented at this Conference :

(1) the energy spectra of proton, helium and iron nuclei fairly well match those measured by the Kascade and Eas-top experiments; (2) the computed knee of the complete spectrum is also in agreement with the experimental data; this agreement is substantiated by the correct bend energy, between $3 - 5 \times 10^{15}$ eV, and the correct spectral index of 3 above 6×10^{15} eV (see figures 11 and 12 and their legends). (3) The positions of the ankles and knees along the energy axis are distinctively and uniquely interconnected by

the average magnetic field strength, which forges the grammage, and by the rate at which inelastic cross sections rise with energy, as shown in figure 15. This fundamental conclusion corroborates the explanation of the knees and ankles described in Section 3 and 4.

It seems to us that the coherent set of observational facts and related physical processes, affecting the propagation of galactic cosmic rays in the disk, as described in Sections 2 and 3, form the irreducible basis for any further quantitative exploration of the knees and ankles of the cosmic radiation. This quantitative exploration is probably feasible using other simulation codes (see, for example, Moskalenko, 1997).

References

- [1] Adams, J. H. et al. (ATIC Coll.): 2005, *ATIC Public Summary*, LSU 10-12-2005.
- [2] Aharonian, M. et al. (HESS Coll.): 2006, *Nature* **439**, 695; Aharonian, M. et al.: 2006, *Astro-ph/0603021*
- [3] Amenomori, M. et al. (Tibet Coll.): 1996, *Astrophysical Jour.* **461**, 408;
- [4] Amenomori, M. et al.: 2000, *Phys. Rev.* **D 62**, 112002.
- [5] Amenomori, M. et al.: 2006, *Physics Letters* **B 632**, 58-64.
- [6] Antoni, T. et al.: 2005, *Astroparticle Physics* **24**, 1.
- [7] Asakimori, K. et al.: 1998, *Astroparticle Physics* **502**, 278.
- [8] Beck, R. et al.: 1980, *Nature* **283**, 272.
- [9] Beck, R. et al.: 1994, *Astronomy & Astrophysics* **292**, 409.
- [10] Beck, R. et al.: 2003, *Astronomy & Astrophysics* **411**, 3.
- [11] Brunetti, M. T. and Codino, A.: 2000, (Paper I) *Astrophysical Jour.* **45**, 138.
- [12] Cherry, M. L.: 1999, *Proc. 26th ICRC, Salt Lake City, Utah*, **Vol. 3**, 187.
- [13] Codino, A., Brunetti M.T. and Menichelli M.: 1995, *Proc. 24th ICRC, Rome*, **Vol. 3**, 100.

- [14] Codino, A. and Plouin F.: 2003, *Proc. 28th ICRC, Tsukuba*, **4**, 410.
- [15] Codino, A.: 2005, *Ultrahigh cosmic rays beyond the ankle are accelerated in the space between galaxies*, Proc. 29th ICRC, Pune, India.
- [16] Codino, A. and Plouin F.: 2006, (Paper III) *Galactic Basins of Helium and Iron around the Knee Energy*, INFN/TC-06/05, February 20, 2006, Frascati, Italy.
- [17] Codino, A. and Plouin F.: 2006, (Paper II) *Astrophysical Jour.* **639**, 173.
- [18] Codino, A. and Plouin F.: 2006, *The origin of the ankle* , **CRIS** 2006 Catania Int. Conference.
- [19] Codino, A.: 2006, *Postulating constant spectral indices for all ions of the cosmic radiation*, in preparation.
- [20] Dar A. et al.: 1998, *Astronomical Journal* **90**, 456.
- [21] Erlykin, A. D.: 1996, in *Frontier Objects in Astrophysics and Particle Physics*, F. Giovannelli & G. Mannocchi (eds.), Italian Physical Society, Editrice Compositori, Bologna, Italy, **57**, 363.
- [22] Gaisser, T. K.: 1990, Cosmic rays and particle physics, Cambridge: *Cambridge University Press*, **236**, 268.
- [23] Giacalone J. and Jokipii J.R.: 1999, *The Astrophysical Jour.* **520**, 204.
- [24] Graeve A. et al.: 1988, *Astronomy & Astrophysics* **192**, 66-76.
- [25] Hara, T., et al. (Akeno Coll.): 1979, *Proc. 16th ICRC, Kyoto*, **Vol. 8**, 175.
- [26] Haungs, A. et al.: 2003, *Report Progress in Physics*, **Vol. 66**, 1145 and, 2004, *Astro-ph/0312295*.
- [27] Hillas A. M.: 1984, *Ann. Review Astronomy and Astrophysics* **22**, 425.
- [28] Hillas A. M. et al.: 1998, *Physics Reports*, **305**, 93.
- [29] Kampert, K. H. et al.: 2003, *Acta Physica Polonica B* **35**, 1799.
- [30] Klein, U. et al.: 1982, *Astronomy & Astrophysics* **116**, 175.

- [31] Klein, U. et al.: 1983, *Astronomy & Astrophysics* **127**, 177.
- [32] Klein, U., Wielebinski R. and Beck R.: 1984, *Astronomy & Astrophysics* **133**, 19.
- [33] Knapic, J. J. et al.: 2000, *Astronomy & Astrophysics* **362**, 910.
- [34] Kulikov, G. V. et al.: 1958, *JEPT* **35**, 635.
- [35] Lawrence, M. A. et al.,(Haverah Park Coll.): 1990, *Proc. 21th ICRC, Adelaide, Australia*, **Vol. 3**, 159; Ave, M. et al.: 2002, *Astro-ph/0112253* (data revision).
- [36] Mathewson, D. S. et al.: 1972, *Astronomy & Astrophysics* **17**, 468.
- [37] Moskalenko I.V., Schoenfelder V. and Strong A. W.: 1997, *Proc. 25th ICRC, Durban, South Africa*, **Vol. 4**, 257.
- [38] Mueller, D.: 1989, *Advances in Space Research*, **Vol. 9, No. 12**, 31.
- [39] Nagano, M. et al. (AGASA Coll.): 1990, *J. Phys. G, Nucl. Phys.* **18**, 423; 1995, Yoshida, S. et al., *Astropart. Phys.* **3**, 105; 2002, Takeda, M. et al., *Astro-ph/0209422* (data revision).
- [40] Navarra, G. et al.: 2003, *Proc. 28th ICRC, Tsukuba*, **Vol. 1**, 147.
- [41] Ondrechen, J. P.: 1985, *Astronomical Journal* **90**, 1974.
- [42] Plaga, R.: 2002, *New Astronomy* **7**, 317.
- [43] Rossi, B.: 1971, in *Raggi Cosmici* , Piccola Biblioteca Einaudi., p. 254 (first english edition 1964).
- [44] Roth, M., et al.: 2003, *Proc. 29th ICRC, Tsukuba*, **Vol. 5**, 305.
- [45] Sofue, Y. et al.: 1980, *Astronomy & Astrophysics* **91**, 335.
- [46] Sofue, Y. and Fujimoto, M.: 1983, *Astrophysics Jour.* **265**, 722.
- [47] Sofue, Y. et al.: 1985, *Astronomy & Astrophysics* **144**, 257.
- [48] Springer R. W. et al. (HiRes Coll.): 2003, *Proc. 28th ICRC Tsukuba*, **Vol. 2**, 256.
- [49] Sukumar, S. and Allen, L. J.: 1991, *Astrophysics Jour.* **382**, 100.
- [50] Vallée, J. P.: 1998, *Fundam. Cosmic Physics* **19**, 319-422.